Active contours in segmentation of fiber like objects

E. Demjénová[1, 2], J. Janáček[3], I. Zolotová[2], Z. Tomori[1]

[1]Department of Biophysics, Institute of Experimental Physics, Slovak Academy of Sciences, Watsonova 47, 043 53, Košice, Slovak Republic

[2]Department of Cybernetics and Artificial Intelligence, Faculty of Electrical Engineering and Informatics, Technical University of Košice, Letná 9, 042 00, Košice, Slovak Republic

[3]Department of Biomathematics, Institute of Physiology, Academy of Sciences of the Czech Republic, Prague, Czech Republic, Vídeňská 1083, 142 20, Praha, Czech Republic

Abstract:One of the most critical steps in the process of digital image analysis is segmentation: separation of an image into regions that have strong correlation with objects of the real world. Segmentation of fiber like objects is a key problem in several image processing application. This paper overviews deformable models, as well as segmentation techniques employed for fiber like objects and propose an algorithm for segmentation of endoplasmatic reticulum using deformable models with automatic initialization.

Keywords: *image segmentation, deformable models, fiber like objects*

1 Introduction

Image segmentation is one of the most important steps leading to the analysis of image data; its main goal is to divide an image into parts that have a strong correlation with objects of the real world. Segmented images are now used in a multitude of different fields, such as industrial, distant reading, biomedical or physical applications. Image segmentation remains a difficult task, however, due to both the variability of object shapes and the variation in image quality. Processed images are often corrupted by noise or sampling artifacts, which can cause considerable difficulties when applying classical segmentation techniques such as edge detection and thresholding. As a result, these techniques either fail completely or require some kind of postprocessing step to remove invalid object boundaries in the segmentation result.

To address these difficulties, *deformable models* have been extensively studied and widely used with promising results. Deformable models are curves or surfaces defined within an image domain that can move a) under the influence of *internal forces*, which are defined within the curve or surface itself, and b) *external forces*, which are computed from the image data. The internal forces are designed to keep the model smooth during deformation. The external forces are defined to move the model toward an object boundary or other desired features within an image. By constraining extracted boundaries to be smooth and incorporating other prior information about the object shape, deformable models offer robustness to both image noise and boundary gaps.

Deformable models have become popular since publishing the work [4] in the late eighties and from that time they have grown to be one of the most active research areas in image segmentation. Various names, such as snake, active contours or surfaces, balloons, and deformable contours or surfaces have been used in the literature to refer deformable models.

Segmentation of *fiber like structures* is a key problem in several image processing and analysis applications. Examples include the detection of roads and valleys in satellite images, visualization of DNA chains using atomic force microscopy, the extraction of blood vessels from retinal, magnetic resonance, computed tomography, or X-ray angiography images for the purpose of quantification or visualization, and the tracing of neurons in three dimensional (3D) confocal microscopy images for histological studies.

The concept of fiber like objects is used intuitively in this paper. They represent a few pixel wide elongated structures, with a circular cross section. They are often ambiguous, such as branching, touching or crossing structures, objects with crooked traces. These defects disable design of fully automatic methods, which leads to using rudimentary techniques, such as manual delineating of objects, which is extremely time consuming process and moreover, their results highly depend on the human operator.

The goal of this paper is to give insight into deformable models and segmentation of fiber like objects, as well as to publish our experiences using active contours in a real application. The paper is organized as follows: sections 2 and 3 describe deformable models and one of their basic formulations, respectively basic segmentation methods of fiber like objects. In section 4 we introduce an application area: segmentation of endoplasmatic reticulum, results are presented in section 5. Finally, we draw conclusions and describe future work.

2 Deformable models

There is described one of the basic formulations for parametric deformable models [4, 14]: *an energy minimizing approach* in this section.

Energy minimizing formulation is based on finding a parametrized curve that minimizes the weighted sum of internal energy and potential energy. The internal energy specifies the tension or the smoothness of the contour. The potential energy is defined over the image domain and typically possesses local minima at the image intensity edges occuring at objects boundaries or ridges.

Mathematically, a deformable contour is a curve $\mathbf{X}(s) = (X(s), Y(s)), s \in [0,1]$, which moves through the spatial domain of an image to minimize the following energy functional:

$$\varepsilon(\mathbf{X}) = S(\mathbf{X}) + P(\mathbf{X}) . \tag{2.1}$$

The first term is the internal energy functional and is defined to be

$$S(X) = \frac{1}{2}\int_0^1 \alpha(s)\left|\frac{\partial \mathbf{X}}{\partial s}\right|^2 + \beta(s)\left|\frac{\partial^2 \mathbf{X}}{\partial s^2}\right|^2 ds . \tag{2.2}$$

The first-order derivative discourages stretching and makes the model behave like an elastic string. The second-order derivative discourages bending and makes the model behave like a rigid rod. The weighting parameters $\alpha(s)$ and $\beta(s)$ can be used to control the strength of the model's tension and rigidity, respectively.

The second term is the potential energy functional and is computed by integrating a potential energy function as the integral of the potential energy function $P(x, y)$ along the contour $\mathbf{X}(s)$:

$$P(\mathbf{X}) = \int_0^1 P(\mathbf{X}(s))ds .$$

The potential energy function is derived from the image data and takes smaller values at object boundaries as well as other features of interest. Given a grey-level image $I(x, y)$ viewed as a function of continuous position variables (x, y), a typical potential energy function designed to lead a deformable contour toward step edges is

$$P(x, y) = -w_e\left|\nabla\left[G_\sigma(x, y) * I(x, y)\right]\right|^2 , \tag{2.2}$$

where w_e is a positive weighting parameter, $G_\sigma(x, y)$ is a two dimensional Gaussian function with standard deviation σ, ∇ is the gradient operator and * is the 2D image convolution operator.

3 Segmentation of fiber like objects

There is a wide range of segmentation techniques that were applied for fiber like objects. They can be classified according to different criteria, e.g. automatic/semiautomatic, the amount of a priori knowledge used by the technique etc. These segmentation methods are divided according to their basic principles in this paper. The given categorization is not the only possible one and individual methods can be classified into more than one class [5].

Pattern recognition techniques deal with the automatic detection or classification of objects or features. Humans are very well adapted to carry out such tasks. Some of these techniques are the adaptation of human ability to the computer systems. Pattern recognition techniques may be divided into next classes: multi-scale approaches, skeleton-based approaches (fig.1), region growing approaches, ridge-based approaches [1] (fig.2), differential geometry-base approaches, matching filter approaches [12], mathematical morphology schemes, e.g. top hat or watershed segmentation.

Model based approaches apply explicit fiber models to extract the scene. The following methods belong into this class: deformable models (both parametric and geometric ones), parametric models, where objects of interest are defined parametrically, e.g. as a set of overlapping ellipsoids and template matching [11]. Parametric deformable models for segmentation of fiber like objects are described in the next section.

Tracking based approaches apply local operators at places known to be an objects and that belong to an object and track it. Tracking starts from an initial point and detects either central line or boundaries by analyzing the pixel orthogonal to the tracking direction.

Artificial intelligence based approaches utilize knowledge to guide the segmentation process and to delineate individual structures. Different types of knowledge are employed in different systems from various sources. One knowledge source is the properties of the image acquisition technique. These systems use low level image processing algorithms, e.g. thresholding and thinning and high level knowledge is used for controlling the process. These methods are accurate, however their computational complexity is much larger than other methods [10].

Neural networks are motivated by biological learning and widely used in pattern recognition. They were employed also in segmentation of fiber like objects [13].

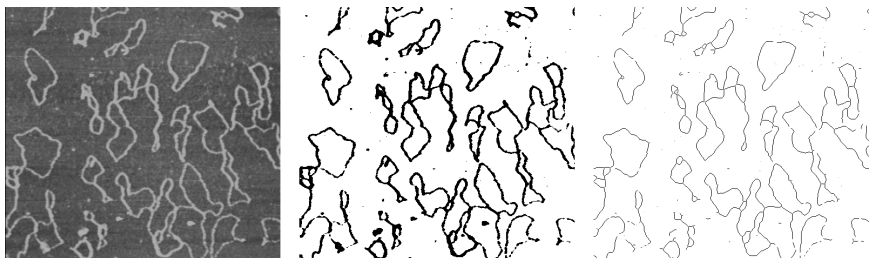

(a) (b) (c)

Fig1. Example of a skeletonization process. (a) atomic force image of a DNA segment, (b) binary image obtained by thresholding, (c) skeleton

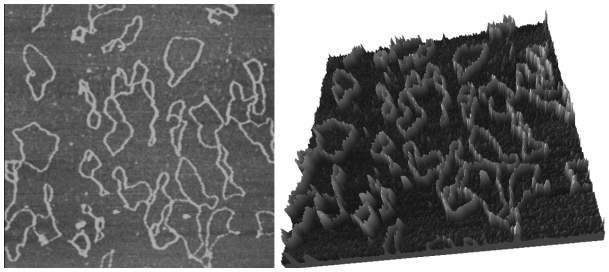

(a) (b)

Fig2. (a) atomic force image of DNA, (b) the corresponding three dimensional intensity height map

3.1 Parametric deformable models in segmentation of fiber like objects

Different modifications of parametric deformable models [4] are often used in segmentation of fiber like objects. Modifications that allow their application in this field mainly deal with topological changes [8], modifying the internal energy, incorporating a priori knowledge into the models and effective initializing of the model.

McInerney and Terzopoulos describe affine cell decomposition-based (ACD) deformable surface and show the potential use of these models in extraction of complex structures from medical image volumes. Topologically deformable ACD-based models, called T-snakes and T-surfaces are parametric models that embed deformable models in an ACD framework to extract very complex structures. 2D

deformable models known as *topologically adaptable snakes*, T-snakes are introduced in [8]. Combinating the ACD framework with deformable models allows to overcome the limitations of classical models while keeping the traditional properties. A T-surface is defined as a closed oriented triangular mesh. The vertices of the triangles act as a dynamic particle system where the particles are connected by discrete springs. As the T-surface moves under the influence of internal and external energy forces, the model is reparametrized with a new set of triangles and nodes from the intersection points of the model with the superposed grid. Reparametrization of the model at every step allows the model topologically transfer and adapt itself to more complex structures.

Different types of deformable models were implemented in segmentation of fiber like objects. In [9] three dimensional deformable model is used for reconstruction of three dimensional paths in angiography. In [3] is described employing of deformable models for detecting rivers in high resolution satellite images.

4 Segmentation of endoplasmatic reticulum

Images of endoplasmatic reticulum of tobacco cells were segmented to extract fiber like structures. The proposed algorithm consists of two steps: automatic initialization provides a reasonable input for the active contour deformation.

4.1 Initialization

Fibrous structures in 2D images were enhanced by scale-space ridge detection [6]. The images were smoothed by Gaussian filter with kernel

$$K_t = \frac{1}{2\pi t} e^{-\frac{x^2+y^2}{2t}} \qquad I_t = I * K_t$$

with values of t equal to 2, 2√2, 4 pixels. Normalized higher eigenvalue of matrix of second derivatives of the image at each degree of smoothing t was calculated by formula

$$\frac{t}{2}\left(\frac{\partial^2 I_t}{\partial x^2} + \frac{\partial^2 I_t}{\partial y^2} + \sqrt{\left(\frac{\partial^2 I_t}{\partial x^2} + \frac{\partial^2 I_t}{\partial y^2} \right)^2 + 4\left(\frac{\partial^2 I_t}{\partial x \partial y} \right)^2} \right)$$

The maximal value from the three resulting images was filtered by morphological opening using the 5 pixel structural element and segmented by thresholding. Voronoi mosaic of the boundary points was constructed using Euclidean distance transform algorithm by [2] and skeleton was generated after [10] from boundaries

between the mosaic cells, and pruned by omitting the branches generated by couples of points whose geodetical distance along the boundary was less then 10 pixels.

4.2 Active contour implementation

A contour is represented as a list of vertices with x, y co-ordinates. The image component of the energy term is calculated for the image pixels corresponding to the contour vertices. Each vertex in this list may be considered as being connected by an edge to the next vertex in the list [3].

An important component of contour models is the *curvature term* in the energy function. We used the actual angles (in degrees) of the contour segments, and the change in this angle at each vertex was used to determine the curvature energy. Equation (4.1) gives the formula used for the angle created by the line segment connecting two points (x_1, y_1 and x_2, y_2). Note that taking the absolute value of the difference between the co-ordinates results in a measure for θ that is in the first quadrant if the angle is being measured from standard positions (the positive x axis). Thus the angles must be adjusted accordingly dependent on which quadrant the line segment will fall in if the first point is located at the origin of the coordinate system

$$\theta = \arctan\left(\left|\frac{y_2 - y_1}{x_2 - x_1}\right|\right). \qquad (4.1)$$

Each vertex has a preceding and subsequent edge segment for which and angle can be calculated (fig.3). The curvature energy is based on the differences between these angles. Due to the manner in which angles are handled, this difference cannot be calculated by simple subtraction of the edge angles. To solve this problem, we used the following technique in calculating the curvature. For two angles a and b, let $m = \max\{a,b\}$ and $s = \min\{a,b\}$, then the difference between a and b can be calculated by

$$\Delta\theta = \min\{m - s, 360 - m + s\}.$$

This angular difference is determined once again for each position in a neighborhood around the current vertex, and these angles are normalized according to the following equation:

$$E_{curv} = \frac{\Delta\theta}{\max\{\Delta\theta\}}$$

where, E_{curv} is the curvature energy, $\Delta\theta$ is the curvature at the vertex position under evaluation, and $\max\{\Delta\theta\}$ is the maximum curvature among the neighbors.

The *image score* is based on the edge strength at the pixel underlying the vertex being evaluated, with low scores representing high intensities. A variable sized neighborhood (set interactively by the user) around each vertex is analyzed to determine the new position of each vertex. Image scores are calculated for each of

the current vertex's immediate neighbors and these values are subsequently translated into energy scores in the <0.0;1.0> range by normalizing each image score by the range of scored within the vertex neighborhood as follows:

$$E_{img} = 1.0 - \frac{(I - min)}{(max - min)},$$

where E_{img} is the image energy score, I is the current image score for the pixel under evaluation, min, is the minimum image score in the neighborhood under evaluation, and max, is the maximum image score in the neighborhood under evaluation.

Within a search neighborhood this method yields a set of scores ranging from <0.0;1.0> for each vertex. However, this same range of scores would be set of each neighborhood, even if there is little variation in image values within the neighborhood, such as might be the case where no ridge is present. Therefore, if $max - 5 < min$, then the value for min is set to $max - 5$, to ensure that low energy scores are not assigned to areas where there is little variation in image intensity.

The *continuity energy* is minimized by maintaining a regular spacing of vertices along the length of the contour. This is important, as the image energy will cause vertices to accumulate along high ridges and leave poor representation in regions of the image where ridges are not so high. As with the image energy score, an initial continuity measure is made for each neighbor of a current vertex, and is then normalized to the <0.0;1.0> range based on the range of values in the neighborhood. The initial score is calculated by

$$S_{cont} = \left| d_{avg} - \left\| v_p - v_c \right\| \right|, \qquad (4.2)$$

where S_{cont}, is the initial continuity score, d_{avg}, is the average distance between vertices on the contour, v_p is the previous vertex, v_c is the current vertex, $\left\| v_p - v_c \right\|$ is the Euclidean distance between v_p and v_c.

The value is normalized by:

$$E_{cont} = \frac{S_{cont}}{\max\{S_{cont}\}}$$

where E_{cont} is the continuity energy score, S_{cont} is the current continuity score for the vertex neighbor under evaluation as calculated in equation (4.2), $\max\{S_{cont}\}$ is the maximum value for S_{cont} among current vertex's neighbors.

The total vertex energy is determined by calculating the weighted average of the three component scores (image, continuity, and curvature).

The contour deformation stage attempts to find a configuration of the contour which minimized the totals of all three energy terms (image, continuity, curvature) for the entire contour. We applied the *Greedy Algorithm*, described in [14], which determined where the current vertex could be repositioned to minimize the total energy. Although the positions of adjacent contour vertices are used in calculating

curvature energy, the influence of the decision regarding current vertex position on the energies of adjacent vertices is not considered. The algorithm calculates the energy score for each image position within a neighborhood surrounding the current vertex, and moves that vertex to the position with the lowest energy score (fig.4).

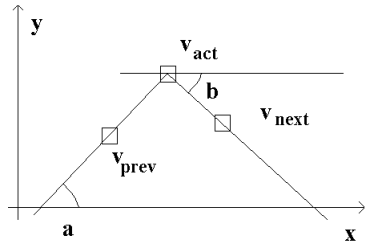

Fig.3 Calculating the curvature in v_{act}, where the preceding edge segment is $v_{act}v_{prev}$ the subsequent edge segment is $v_{next}v_{act}$.

(a) (b) (c)

Fig.4 Repositioning a vertex using the Greedy Algorithm (a) original position, (b)energy values for each neighbor (c) repositioned vertex

5 Experiments

The described technique was implemented in the Microsoft Visual C++ 6.0 programming environment. After initial experimentation the parameters were fixed to: σ =1.3 for Gaussian smoothing, weighting parameter for the external force = 0.75, weighting parameter for the curvature term = 0.125, weighting parameter for the continuity term = 0.125, neighborhood window size of 5x5pixels. Accuracy was evaluated visually. Fig.5 gives an impression of the results of the initialization process (b), (c) and the active contour deformation process (d).

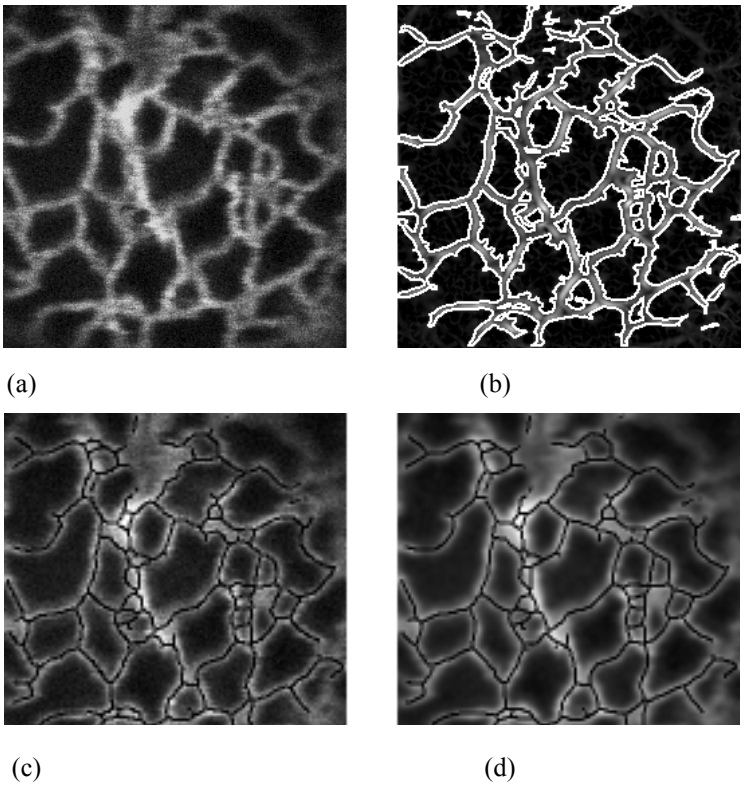

Fig5: (a) fluorescence image of endoplasmatic reticulum of GFP transformed tobacco cell, (b) thresholded image enhanced by scale-space ridge detection filter, (c) skeletonized image, (d) Gaussian smoothed image with skeleton regularized by active contour model

Conclusions

Deformable models are a powerful tool for image segmentation and boundary extraction, particularly in corrupted images or in objects that contain boundary gaps. However, they require user interaction or interaction with some higher-level image understanding process. This interaction must specify an approximate shape and starting position for the model somewhere near the desired contour. Moreover, the model may need other accessory information, such as setting a) parameters of the energy functional, defined by equations (2.1) and (2.2) or b) size of the neighborhood defined in the section 4.2. In this work we used experimentally set constant values. Future work in this field assumes designing a more sophisticated method for adjustment of these values, which are not necessarily be the same for different applications.

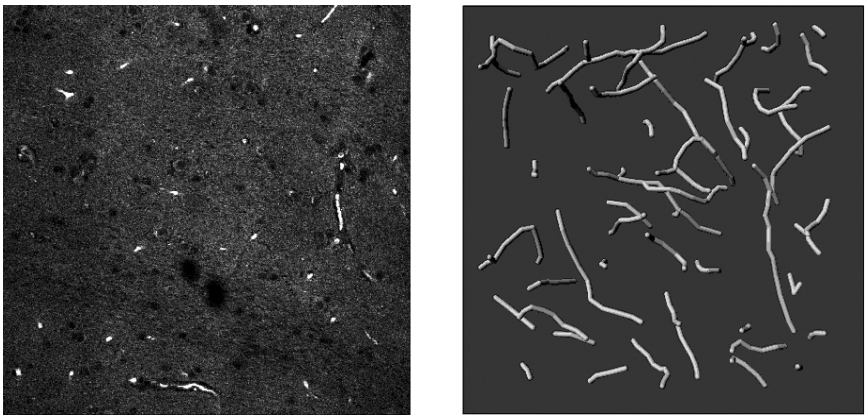

(a) (b)

Fig6. (a) original white matter sample, (b) cylindrical model of manually traced microvessels

Results were evaluated visually. Although these were promising, for further testing it will be necessary to develop an accurate model of these biological structures, similar to that presented in [7].

Another future work would be enhancing the automatic initialization process and active contour implementation into three dimensions. Such an application, illustrated in the fig.6, is a segmentation of capillaries from rat brain white matter, and its subsequent qualitative and quantitative analysis.

Acknowledgements

We thank B. Radochova, Institute of Physiology ASCR, Prague, and K. Schwarzerova, Faculty of Natural Sciences, Charles university, Prague for images of endoplasmic reticulum, Dr. J. Archambeau and Dr. X.W. Mao, Loma Linda Hospital, for images of brain capillaries and Prof. G. Dietler, University of Lausanne, for image of DNA.

Support of grants from Slovak Grant Agency VEGA No. 2/5048/25, 1/2185/05, by Ministry of Education of the Slovak Republic, grant of the Academy of Sciences B6011309, grant of Ministry of Education, Youth and Sport of the Czech Republic and Ministry of Education of the Slovak Republic KONTAKT 139 are acknowledged.

References

[1] S.R. Aylward, "Initialization, noise, singularities, and scale in height ridge traversal for tubular object centerline extraction," *IEEE Trans. Med. Imag.*, vol.21, no.2, pp.61-75, 2002.

[2] H. Breu, J. Gil, D. Kirkpatrick, M. Werman, "Linear Time Euclidean Distance Transform Algorithms," *IEEE Trans. Patt. Anal. Mach. Intell.*, vol.17 , no.5, Pages: 529-533, 1995.

[3] C.R. Dillabaugh, K.O. Niemann, and D. Richardson, "Semi-automated extraction of rivers from digital imagery," *GeoInformatica*, vol.6, no.3, pp.263-284, 2002.

[4] M. Kass, A.Witkin, and D. Terzopoulos, "Snakes: active contour models," *Int´l J. Comp. Vis.*, vol.1, no.4, pp. 321-331, 1987.

[5] C. Kirbas and F.K.H. Quek, "Vessel extraction techniques and algorithms: a survey,", in *Proc. IEEE Symposium on Bioinformatics and Bioengineering*, 238, 2003.

[6] T. Lindeberg, "Edge detection and ridge detection with automatic scale selection," *Int'l J. Comp. Vis.*, vol.30, no.2, 117-156, 1998.

[7] J. Marek, E. Demjénová, Z. Tomori, J. Janáček, I. Zolotová, F. Valle, M. Favre, G. Dietler, „Interactive measurement and characterization of DNA confirmation by analysis of AFM image", accepted in *Cytometry*

[8] T. McInerney, and D. Terzopoulos, "T-snakes: Topology adaptive snakes," *Med. Imag. Anal.*, vol.4, no.2, pp.73-91, 2000.

[9] C. Molina, G. Prause, P. Radeva, and M. Sonka, "3-d catheter path reconstruction from biplane angiograms," in *SPIE*, vol.3338, pp.504-512, 1998.

[10] R. Ogniewicz, and M. Ilg, "Voronoi Skeletons: Theory and Applications," *Proc. CVPR'92*, Champaign, Illinois, 63-69, June 1992

[11] U. Rost, H. Munkel, and C.-E. Liedtke, "A knowledge based system for the configuration of image processing algorithms," *Fachtagung Informations und Mikrosystem Technik*, March, 1998.

[12] Y. Sato, S. Nakajima, N. Shiraga, H. Atsumi, S. Yoshida, T. Koller, G. Gerig, and R. Kikinis, "3d multis-scale line filter for segmentation and visualization of curvilinear structures in medical images," *IEEE Medical Image Analysis*, vol.2, pp.143-168, June, 1998.

[13] S. Shiffman, G.D. Rubin, and S. Napel, "Semiautomated editing of computed tomography sections for visualization of vasculature", vol.2707, *SPIE*, 1996.

[14] D.J. Williams and M. Shah, "A fast algorithm for active contours and curvature estimation," *CVGIP:Imag. Under.*, vol.55, no.1, pp.14-26, 1992.

[15] C. Xu, D.L. Pham, J.L. Prince, "Medical image segmentation using deformable models," *Handbook of Medical Imaging, vol.2, Medical Image Processing and Analysis*, pp.129-174, 2000.